Available online at www.sciencedirect.com

ScienceDirect

Energy Procedia 4 (2011) 2192–2199

Energy Procedia

www.elsevier.com/locate/procedia

GHGT-10

Carbonated Water Injection (CWI) – A Productive Way of Using CO2 for Oil Recovery and CO2 Storage

Mehran Sohrabi[1], Masoud Riazi, Mahmoud Jamiolahmady, Nor Idah Kechut, Shaun Ireland and Graeme Robertson

Institute of Petroleum Engineering, Heriot-Watt University, Edinburgh, Scotland, UK

Abstract

The main advantage of CO2 is that at most reservoir conditions it is a supercritical fluid which is likely to develop miscibility with the oil. In reservoirs that miscibility cannot be achieved, CO2 injection can lead to additional oil recovery by mixing with the oil and favourably modifying the flow properties of the oil. Displacement and recovery of oil by CO2 injection has been studied and applied in the field extensively in the past three decades. Concerns over the environmental impact of CO2 have led to a resurgence of interest in CO2 injection in oil reservoirs. The injection of CO2 can enhance oil recovery from these reservoirs and at the same time help mitigating the problem of increased CO2 concentrations in the atmosphere by storing large quantities of CO2 for a long period of time.

CO2 injection projects so far have been mainly limited geographically to oil fields located in areas where large quantities of CO2 have been available mainly from natural resources. Various CO2 injection strategies e.g. cyclic injection, continuous CO2 flood, alternating (WAG) or simultaneous injection of CO2 and water have been applied in these fields. With the new global interest in CO2 injection, many other reservoir settings and scenarios are being considered for CO2 injection in oil reservoirs. This may require injection strategies other than those conventionally used for CO2 injection especially for offshore reservoirs or in cases where the supply of CO2 can be variable or limited.

An alternative CO2 injection strategy is carbonated (CO2-enriched) water injection. In carbonated water, CO2 exists as a dissolved phase as opposed to a free phase eliminating the problems of gravity segregation and poor sweep efficiency, which are characteristics of a typical CO2 injection project. In fact, both viscosity and density of water increase as a result of the dissolution of CO2 in water. In terms of CO2 storage, through carbonated water injection, large volumes of CO2 can be injected into the reservoir without the risk of leakage of CO2 through caprock.

Using the results of a series of high-pressure flow visualisation experiments, we reveal the underlying physical processes taking place during CWI. The results show that CWI, compared to conventional water injection, improves oil recovery in both secondary (pre-waterflood) and tertiary (post-waterflood) injection modes. Several key mechanisms taking place at the pore level during CWI leading to additional recovery are presented and discussed. Both conventional (light) oil and viscous oil was used in the experiments.

Keywords: CO2 Storage, CO2 Enhanced Oil Recovery, Carbonated Water Injection

* Corresponding author
Email Author: mehran.sohrabi@pet.hw.ac.uk

doi:10.1016/j.egypro.2011.02.106

1. Introduction

With the continued increase in the fossil fuels demand for many years to come [1], there is an inevitable undesired CO_2 emission from the burning of the fossil fuels, which is believed to have contributed to the problem of global warming. One of the important, immediately available and technologically feasible strategies for achieving substantial reductions in anthropogenic CO_2 emissions levels while enabling continued use of existing energy supply is the capture of this CO_2 and its subsequent storage in geological formations such as deep saline aquifers, depleted oil and gas reservoirs and un-mineable coal beds [2]. Injection of CO_2 into depleting oil reservoirs to improve oil recovery has been implemented in many reservoirs worldwide for more than 30 years particularly in the United States where abundant natural resources of CO_2 is available [3]. In these conventional CO_2 EOR projects, maximizing the oil recovery is the main objective while CO_2 injection and sequestration are to be minimized as much as possible.

In the coupled CO_2 EOR and storage projects, the main objective is no longer just maximizing the oil recovery but also maximizing the amount of CO_2 stored in the reservoir at the end of the process. There are just limited numbers of successful field scale CO_2 EOR implementations using anthropogenic CO_2; example of which are Weyburn-Midale project [4], Salt Creek [5], Rangely Weber Unit [6], Daqing and Liaohe [7]. The most likely source of the anthropogenic CO_2 is from the coal fired plants which contribute approximately 40% of the total CO_2 emission [8]. The high cost associated with the capture of CO_2 from these plants, its pressurization and transport [9] and location that is normally far from the oil fields is however unlikely to make conventional CO_2 flooding, which requires continuity and security of the CO_2 supply, using this anthropogenic CO_2 economical. Yet, there are also smaller sources of this anthropogenic CO_2 that would contribute to the CO_2 emission, which might be located closer to the candidate fields, such as from CO_2 separation from natural gas or associated gas or downstream activities e.g. refineries and petrochemicals plants at much lower price.

An alternative injection strategy in which CO_2 is used more efficiently (compared to conventional CO_2 injection) is carbonated water injection (CWI). This process is particularly attractive for offshore oil reservoirs or other reservoirs with limited access to CO_2. It could also serve as a water-based EOR method for watered-out oil reservoirs in which high water saturations adversely affects the conventional CO_2 injections. Dissolving this anthropogenic CO_2 into the injected water for otherwise plain waterflooding would contribute in reducing the CO_2 emission to the environment. For CO_2 storage, CWI eliminates the risk of buoyancy-driven leakage as in the case of bulk phase injection [10] since CO2 is in solution rather than a free phase and since carbonated water is denser than the native brine [11], thus securing storage and reducing the cost of monitoring the stored CO_2.

In CWI, CO_2 is dissolved in water and transported through the reservoir by the flood water. At typical pressure and temperature of oil reservoirs, CO_2 solubility could be, for example, as high as 30 Sm3/m3 (168 Scf/bw), much higher than hydrocarbon gases, which is favourable for oil recovery and beneficial for CO_2 storage. As a single phase, carbonated water mobility contrast with oil is more favourable than in the CO_2 gas-oil system. CO_2 is more evenly distributed within the reservoir thus retards CO_2 breakthrough and improves sweep efficiency.

The objective of the ongoing Carbonated Water Injection JIP (joint industry project) at Heriot-Watt University is to investigate the application of CO2-enriched water injection as an injection strategy for enhanced oil recovery and CO2 storage using an integrated experimental and theoretical approach. In this paper we present some of the results of four direct flow visualisation experiments which were carried out as part of a comprehensive series of experiment that are being performed in this project.

2. Experimental Setup and Procedures

Flow Visualisation Equipment

A high-pressure micromodel rig, capable of operating at pressures as high as 5000 psia, was used in the flow visualization experiments. Micromodels are transparent porous media allowing direct observation of pore-scale mechanisms of fluid displacement and recovery under various injection scenarios and conditions.

A two-dimensional pore structure is etched onto the surface of a glass plate, which is otherwise completely flat. A second glass plate is then placed over the first, covering the etched pattern and thus creating an enclosed pore space. This second plate, the cover plate, has an inlet hole and an outlet hole drilled at either end, allowing fluids to

be displaced through the network of pores. Because the structure is only one pore deep, and the containing solid walls are all glass, it is possible to observe the fluids as they flow along the pore channels and interact with each other. It is also possible to observe how the geometry of the pore network affects the patterns of flow and trapping. High-pressure micromodel rigs have been extensively used in our research group and the details could be found in previous publications [12]. In this study a water-wet micromodel with a geometric pore pattern was used. The basic characteristics of the micromodel are shown in Table 1.

Table 1: Dimensions of the micromodel used.

Height, cm	Width, cm	Pore Volume, cc	Ave. Pore depth, mm	Pore dia. Range, mm
4	0.7	0.01	50	30-500

Fluids

The fluid system used in the experiments consisted of two different types of oil (n-Decane and a viscous mineral oil), distilled water and carbon dioxide. The viscosity of the mineral oil at atmospheric pressure and the temperature of the experiments, 311 K (38°C), was 16.5 mPa.s (cP) whereas the viscosity of n-Decane, which was used as a lighter oil compared to the mineral oil, was 0.83 mPa.s (cP) at 13.8E5 Pa (2000 psia) and 311 K (38°C) [13]. Carbonated water was prepared by mixing degassed water with pure CO2 in a rocking cell at 311 K (38°C) and 13.8E5 Pa (2000 psia). To distinguish between the oil and the aqueous phase, the colour of the water was changed to blue by adding a water-soluble (0.6% wt/wt) blue dye.

3. Results and Discussion

Micromodel Experiments

In the tests reported here, to minimise the gravity effect, the micromodel was mounted horizontally. Figure 1 shows the micromodel at the beginning of a typical test when fully saturated with blue water. The Figure shows the pore pattern as well as the triangles at either end of the porous section, which have been designed to evenly distribute the fluids in the porous medium. Figure 2 shows a section of the micromodel at higher magnification to show in more details the pore pattern of the micromodel used in this study. In both of these Figures, the blue areas represent the pores and the white areas are unetched glass representing rock grains. The dimensions of the porous section as well as the size of the pores are given in Table 1. The experiments commenced by saturating and pressurising the micromodel with water. Then, to simulate the primary drainage of water and the initial migration of oil in a reservoir, the oil phase was injected at a very slow rate of 0.1 cm^3 h^{-1} from one end of the horizontal micromodel. The injection of oil stopped when the oil front reached the other end of the micromodel.

Two experiments are reported here. One with n-decane representing a light oil and the other one with a viscous oil with the aim of investigating oil recovery mechanisms during CWI for different oil types.

Light Oil Recovery by CWI

Figure 3, shows fluid distribution in a section of the micromodel at the end of the oil (n-decane) injection period at the beginning of the test. To better differentiate between the unetched glass and the oil, in this image and the following ones, the unetched glass has been shown as hatched areas. Figure 3 shows the relative position of the wetting phase (blue water) and non-wetting phase (n-decane) in the porous medium. Glass is water-wet and as a result, the water in the micromodel occupies the smaller and dead-end pores and also as layers on the walls of the oil-occupied pores. The shape and the direction of the water-oil interfaces are also good indications of water-wet conditions of the micromodel.

After establishing the initial oil and water saturations, water was injected into the micromodel at a low rate of 0.01 cm^3 h^{-1} corresponding to a superficial velocity of 0.7 md^{-1} and an actual (pore) velocity of around 3 md^{-1}. The actual velocity was estimated from the time it took for the water front to travel the length of the micromodel during water injection. Figure 4 illustrates the distribution of oil and water after water flooding. As can be seen, water has displaced part of the oil and has left behind some oil in the form of isolated oil ganglia. The oil production during water flooding took place mainly before the water breakthrough (BT). After BT, the flood water passed through the porous medium via the water films that already had been formed and left the model without any further oil recovery or fluid distribution. The displacement of oil by water during water flooding happened by film flow as well as piston

type displacement. The water films surrounding the oil were observed to become progressively thicker as the water injection progressed and eventually caused disconnection of the oil by snap-off mechanism. The arrow in Figure 4 shows an isolated oil ganglion and the narrowing of oil, which caused by film flow displacement mechanism.

The saturation of the oil in the whole of the micromodel at various stages of the tests was estimated by measuring the number of pixels making the area of the oil divided by the total pore area of the micromodel. Since the depth of all pores in are the same, area ratio is equal to volume ratio. The error in the reported values of saturation is estimated to be +/-10%. The estimated data show that as a result of the first water injection period, the initial oil saturation reduced from 67% to 49%, which showed 18% oil production corresponding to a 26.9% oil recovery factor.

After establishing residual oil saturation by water flooding, CW (carbonated water) injection began with the direction of flow being the same as the preceding water flood and with the same rate of injection (0.01 cm^3 h^{-1}). When CW came in contact with oil and water in the micromodel, partitioning of CO2 from CW and its diffusion and dissolution into the oil phase took place. As a result, the isolated oil ganglia (Figure 4) swelled and consequently displaced some of the aqueous phase from the pores which led to reconnection of some of the isolated oil ganglia which were formed in the previous water flooding. The amount of oil swelling, which is a function of the oil type and CO2 concentration in the CW, controls the coalescence mechanism of the disconnected oil ganglia. During the CWI in this test significant swelling and coalescence of the trapped oil (n-decane) and its subsequent mobilisation and recovery was observed. The additional oil recovery took place gradually during the course of CWI. Figure 5 shows a snapshot of a section of the micromodel at the end of CWI.

Comparison of Figure 5 with Figure 4 shows significant changes in fluid distribution within the micromodel caused by carbonated water injection including oil swelling and coalescence and displacement of the oil and water in the dead end pores. In this Figure, the red arrow points at an example of swelling of an oil ganglion and the green arrow (on the left hand side of the picture) shows the displacement of water from some dead-end pores as a result of the oil swelling. The displacement of water from the dead-end pores could only happen by counter current flow of oil and water which indicates that the swelling of the oil provided enough energy to overcome capillary forces in these pores. Favourable changes in interfacial tension [14] and wettability [15] during dissolution of CO2 can facilitate these displacements. The oval shape in Figure 5 shows an example of coalescence of the disconnected oil ganglia as a result of the oil swelling and water displacement. The rectangular shape shows the disconnection of an oil ganglion due to the oil displacement and its recovery. The saturation of the oil (mixture of oil and CO2) in the micromodel at the end of CWI period was estimated at 64%, which was very close to the initial (before water flood) oil saturation of 67%.

After the CWI period, since the remaining oil was a mixture of the oil and CO2, (plain) water was injected into the micromodel to strip CO2 from oil. This second water injection (WI) period was carried out to obtain the equivalent dead-oil volume of the oil remaining in porous medium after CWI in order to obtain the actual oil recovery due to CWI. The dead-oil saturation and distribution at the end of the second WI period is shown in Figure 6. Comparison of Figure 6 with Figure 5 clearly shows significant reduction in the oil volume and fragmentation due to shrinkage caused by stripping the dissolved CO2. Comparison of fluid saturation after the first WI (Figure 4) and the second WI (Figure 6) reveals that significant additional oil recovery took place during CWI which had been carried out after the first WI. The oil saturation at this point was estimated at 33%, which indicates 16% additional oil production. In other words, 32.7% of the oil which had been left behind after the initial water flooding had been recovered during the CWI period.

Heavy Oil Recovery by CWI

This experiment was carried out to investigate the performance of CWI in viscous oil and to compare the results with the observations made in the light oil (n-decane) experiment. The viscous oil used in the experiment was a hydrocarbon based refined oil with an initial viscosity of 16.5 cP at the conditions of the experiment. For consistency, the same micromodel and aqueous phase was used and the experiment was carried out under the same conditions of pressure and temperature as the previous light oil experiment.

The test started with an oil injection period in the water-saturated micromodel to establish the initial oil and water saturations. Figure 7 shows fluid distribution after the oil injection stage. Comparison of the initial oil saturation and distribution of viscous oil in this test (Figure 7) with its corresponding stage in light oil (Figure 3) shows a very similar fluid distribution and saturation within the micromodel. Nevertheless, a higher initial oil saturation value was achieved in this test (76.4 %) compared to the light oil test (67 %) mainly due to a 20 times

increased in the oil viscosity. After establishing the initial oil and water saturations, an initial water injection was carried out with the same injection rate as the previous test, 0.01 cm^3 h^{-1}. Figure 8 shows the distribution of viscous oil and water after this initial water injection. Comparison of fluid distribution in Figures 7 and 8 shows some viscous oil displacement and recovery due to waterflooding. Water injection resulted in larger trapped oil ganglia after WI in the viscous oil (Figure 8) compared to light oil (Figure 4). Around 19.7% of the oil was recovered during this stage leaving behind 56.7% trapped in the porous medium, compared to 49% water flood residual oil saturation in the light oil experiment. After this initial WI (water injection), CW was injected through the micromodel at a rate of 0.01 cm^3 h^{-1}. Figure 9 shows the fluid distribution in a section of the micromodel at the end of CWI.

During CWI, the viscous oil was observed to swell as CO2 departed from the flowing CW and dissolved in the oil. Comparison of fluid distribution, the sizes and the shapes of the oil ganglia in Figure 9 with Figure 8 clearly shows swelling of the viscous oil during CWI. The arrow in Figure 9 shows an example of an isolated oil ganglion, which has swollen compared to its size in Figure 8. This swelling caused oil reconnection followed by remobilisation and recovery of some of the trapped oil. The red rectangle in Figure 9 illustrates an obvious oil displacement when compared with the same spot in the micromodel after WI period (Figure 8). The amount of the oil swelling observed in the viscous oil case was less than the light oil and hence less oil reconnection and remobilisation took place during viscous oil test. This was mainly due to the fact that CO2 solubility in oil reduces as the oil viscosity increases.

At the end of CWI, the saturation of the remaining oil (mixture of viscous oil and dissolved CO2) was estimated to be 61.4%. Similarly to the light oil experiment, in this experiment again a second water injection period was carried out after CWI in order to slowly strip the dissolved CO2 from the oil and obtain the dead-oil saturation.

Figure 10 shows the dead oil at the end of the second water injection period. Comparison of Figure 10 (2nd WI) with Figure 8 (1st WI) shows significant difference in fluid distribution and saturation as a result of the CWI period. The red rectangle in Figure 10 highlights that a previously large trapped oil ganglion remaining after the initial water injection period (shown by the arrow in Figure 8) has now have a smaller volume (oil production) as well as being broken into several pieces. The residual oil saturation in this stage estimated to be 50%, which shows 6.7% PV additional oil production corresponding to 11.8% recovery from the waterflood residual oil.

Comparison of Figure 6 and Figure 5 with their corresponding stages in the viscous oil (Figure 9 and Figure 10) reveals much higher shrinkage of the oil after striping the dissolved CO2 in the case of light oil (n-decane) compared to what was observed for the viscous oil. The number of oil ganglia in the micromodel after the second WI in the light oil test (Figure 6) was about 50, however the corresponding number for the viscous oil test was just about 15. This difference confirms higher light oil shrinkage as a result of the stripping of the dissolved CO2 which, as expected, indicate higher CO2 solubility for the light oil.

4. Light Oil versus Viscous Oil

Two main mechanisms of oil recovery during carbonated water injection are; oil swelling and subsequent flow diversion and coalescence of the trapped oil ganglia, and the reduction in oil viscosity. The former is the dominant mechanism in light oil due to higher CO2 solubility and the latter is more relevant to viscous oil due to significant reduction in viscosity of these oils as a result of CO2 dissolution.

Figure 11 and Figure 12 show a summary of the oil saturation data estimated at the end of various stages of the experiments with the corresponding recovery factors. The data show that for both n-decane (light oil) and the viscous oil, the injection of carbonated water resulted in more oil recovery over and on top of what had already been recovered during water flooding. However, recovery factor for n-decane (32.7%) was much more than the viscous oil (11.8%). The higher oil recovery observed during the light oil CWI experiment is mainly attributed to the observed higher oil swelling and coalescence in this oil compared to the viscous oil. The Oil swelling factor can be calculated for the whole of micromodel using the oil saturation values at the end of the CW and the second WI periods. Based on the data plotted in Figures 11 and 12 the swelling factor of the light oil is about 94% and the corresponding value for the viscous oil is about 23%. The higher swelling factor for n-decane compared to the viscous oil is consistent with the expected higher CO2 solubility in the lighter oil.

5. Conclusions

The following conclusions can be drawn based on the results of the experiments discussed in this paper:

- CWI as tertiary recovery method (post waterflood) increased oil recovery both for light and the viscous oil. However this increase was higher for the light oil than the viscous oil. This was mainly due to a higher swelling factor in the light oil.
- Two main observed mechanisms of oil recovery during carbonated water injection were; the swelling and subsequent coalescence of trapped oil ganglia, local flow diversion and reduction of the oil viscosity.
- Significant oil swelling was observed. The swelling of the viscous oil and n-decane as a result of partitioning of CO_2 from carbonated water and its dissolution in the oil, were estimated to be 23% and 105%, respectively.

6. Acknowledgements

The Carbonated Water Injection JIP at Heriot-Watt University is equally sponsored by the UK Department of Energy and Climate (DECC), Total, Petrobras, Dong Energy and Statoil which is gratefully acknowledged.

6. References

[1] International Energy Annual 2006, http://www.eia.doe.gov/iea/overview.html, accessed 19th February 2009.
[2] IPCC Fourth Assessment Report Working Group III, 2007. Climate Change 2007: Mitigation of Climate Change in: Metz, B., Davidson, O.R., Bosch, P.R., Dave, R., Meyer, L.A. (Eds), Cambridge University Press, Cambridge, United Kingdom.
[3] 2008 Worldwide EOR Survey, Oil & Gas Journal, April 2008, Volume 106, Issue 15.
[4] Preston, C. et al. 2005. IEA GHG Weyburn CO_2 monitoring and storage project, Fuel Processing Technology, 86, 1547-1568.
[5] Anadarko,"Enhanced Oil Recovery", Anadarko website, accessed August 2010.
[6] National Energy Technology Laboratory, U.S. Dept. of Energy, http://www.netl.doe.gov/technologies/carbon_seq/database/index.html, accessed August 2010.
[7] IEA/CSLF Report to the Muskoka 2010 G8 Summit, Carbon Capture and Storage Progress and Next Steps, 2010
[8] World Energy Outlook 2009 fact sheet, International Energy Agency, http://www.worldenergyoutlook.org/docs/weo2009/ fact_sheets_WEO_2009.pdf
[9] Bachu, S. 2008. CO_2 storage in geological media: Role, means, status and barriers to deployment. Progress in Energy and Combustion Science, 34, 254-273.
[10] Burton, M. and Bryant, S. L. 2007. Eliminating Buoyant Migration of Sequestered CO_2 through Surface Dissolution: Implementation Costs and Technical Challenges, Paper presented at SPE Annual Technical Conference and Exhibition. Anaheim, California, U.S.A.
[11] Hebach A. et al. 2004. Density of Water + Carbon Dioxide at Elevated Pressures: Measurements and Correlation, J. Chem. Eng. Data, 49, 950-953.
[12] Sohrabi, M., Tehrani, D. H., Danesh, A. and Henderson, G. 2004. Visualisation of Oil Recovery by Water-Alternating-Gas Injection Using High-Pressure Micromodels. SPE Journal.
[13] Lemmon E.W., McLinden M.O. and Friend D.G. 2005.Thermophysical Properties of Fluid Systems in NIST Chemistry WebBook, NIST Standard Reference Database No. 69, Eds. P.J. Linstrom and W.G Mallard, National Institute of Standards and Technology (http://webbook.nist.gov).
[14] Daoyong Y., Paitoon T., and Yongan G.: "Interfacial Tensions of the Crude Oil + Reservoir Brine + CO_2Systems at Pressures up to 31 MPa and Temperatures of 27 °C and 58 °C'', Journal of Chemical and Engineering Data, Vol. 50, No. 4, 2005.
[15] Chiquet, P. and Broseta, D.: ''Capillary Alteration of Shaly Caprocks by Carbon Dioxide'', SPE 94183, 2005.

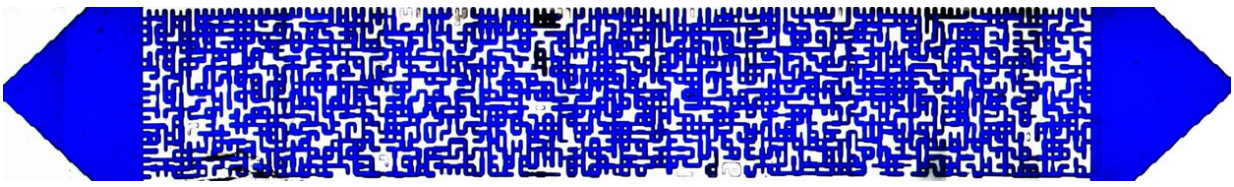

Figure 1: Image of the micromodel when fully saturated with blue-dyed water.

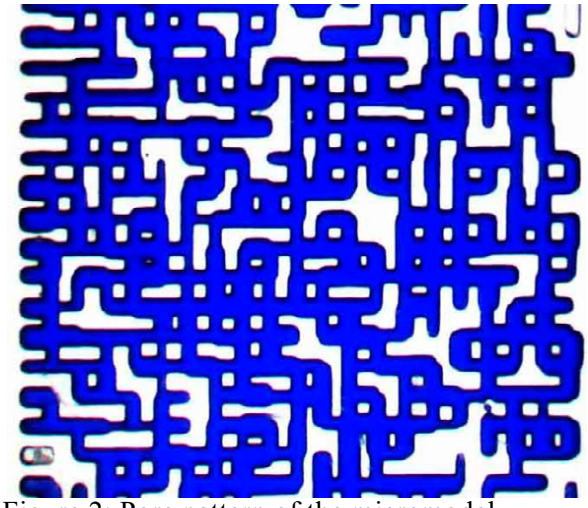

Figure 2: Pore pattern of the micromodel.

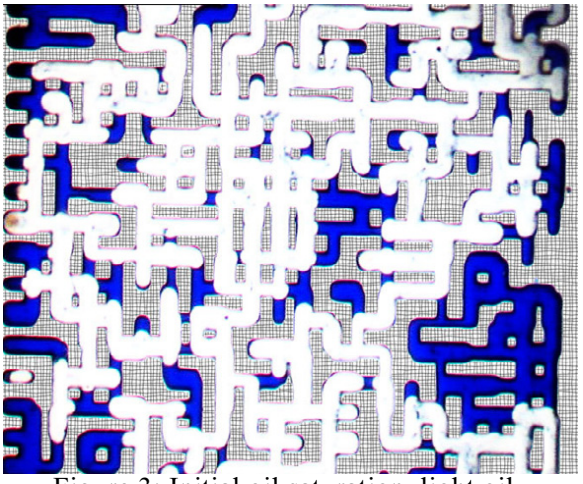

Figure 3: Initial oil saturation, light oil.

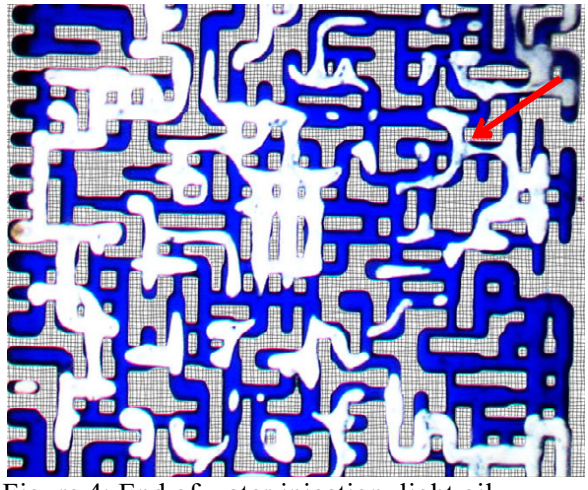

Figure 4: End of water injection, light oil.

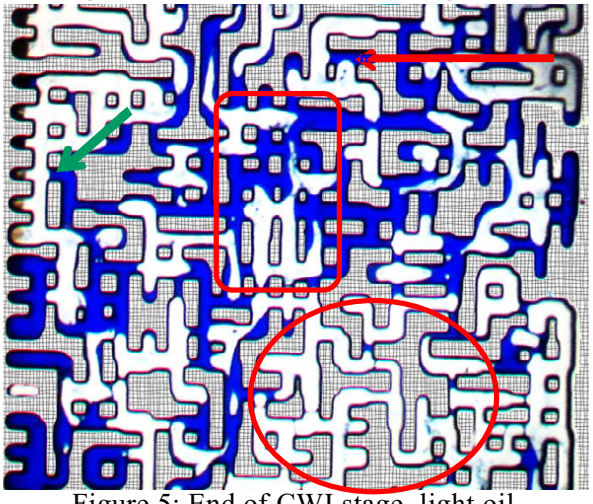

Figure 5: End of CWI stage, light oil.

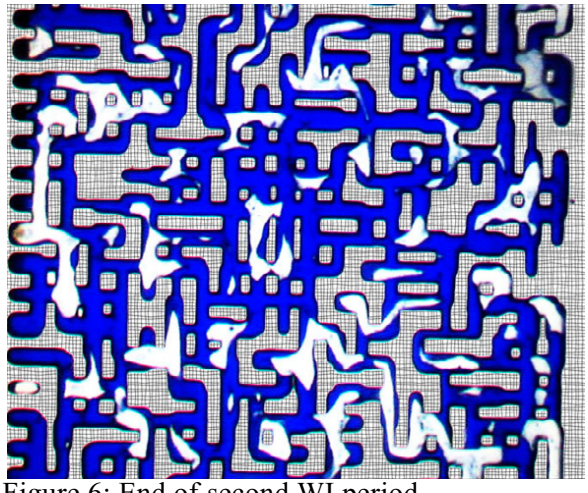

Figure 6: End of second WI period.

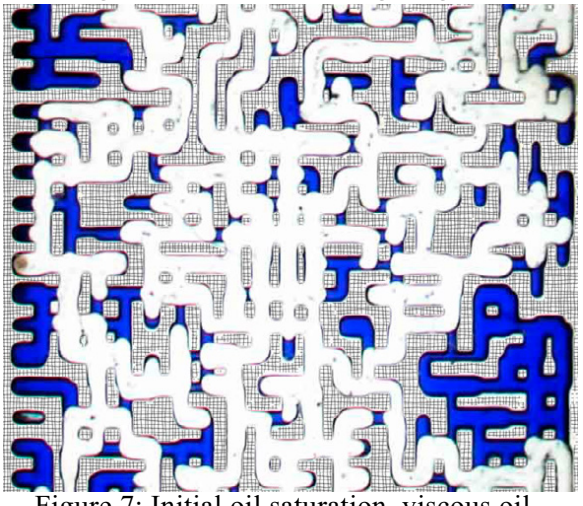

Figure 7: Initial oil saturation, viscous oil.

Figure 8: Fluid distribution after the first WI, viscous oil.

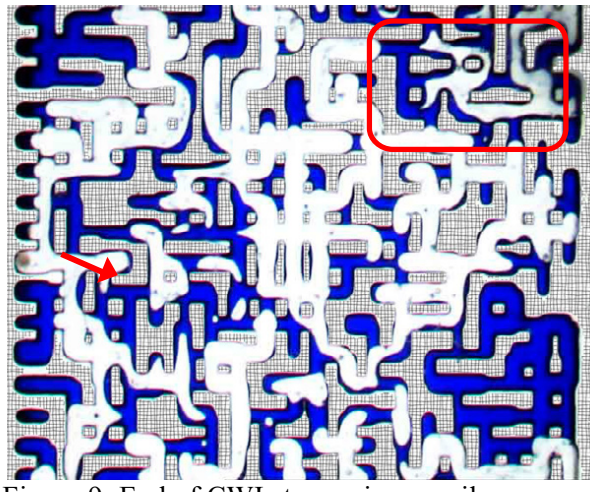

Figure 9: End of CWI stage, viscous oil.

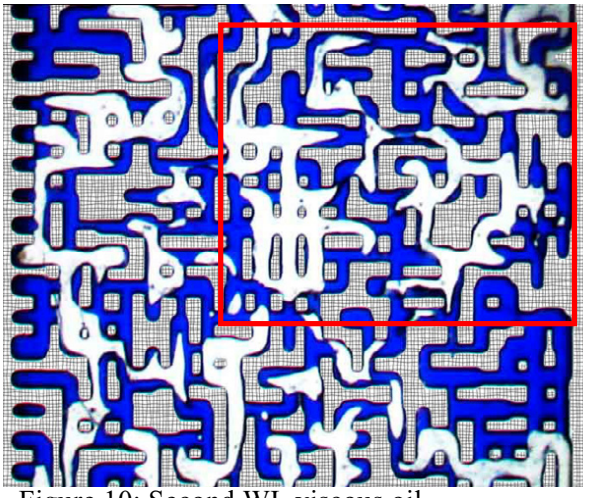

Figure 10: Second WI, viscous oil.

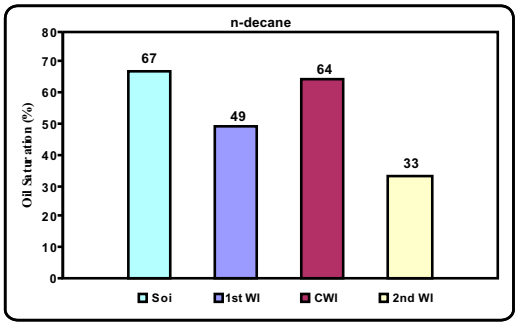

Figure 11: Oil saturation in the first test.

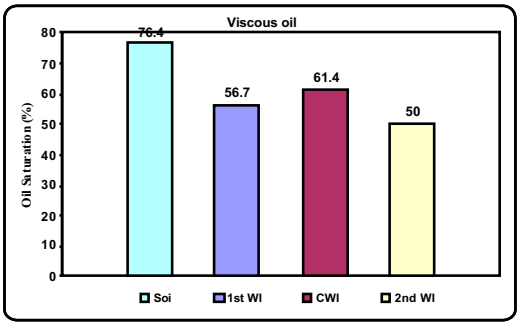

Figure 12: Oil saturation in the second test.